PAPER

Design of a TiO$_2$ nanosheet/nanoparticle gradient film photoanode and its improved performance for dye-sensitized solar cells

Wenguang Wang,* Haiyan Zhang,* Rong Wang, Ming Feng and Yiming Chen

A TiO$_2$ film photoanode with gradient structure in nanosheet/nanoparticle concentration on the fluorine-doped tin oxide glass from substrate to surface was prepared by a screen printing method. The as-prepared dye-sensitized solar cell (DSSC) based on the gradient film electrode exhibited an enhanced photoelectric conversion efficiency of 6.48%, exceeding that of a pure nanoparticle-based DSSC with the same film thickness by a factor of 2.6. The enhanced photovoltaic performance of the gradient film-based DSSC was attributed to the superior light scattering ability of TiO$_2$ nanosheets within the gradient structure, which was beneficial to light harvesting. Furthermore, the TiO$_2$ nanosheets with exposed {001} facets facilitated the electron transport from dye molecules to the conduction band of TiO$_2$ and further to the conductive glass. Meanwhile, the high specific surface area of TiO$_2$ nanosheets helped the adsorption of dye molecules, and the TiO$_2$ nanoparticle underlayer ensured good electronic contact between the TiO$_2$ film and the fluorine-doped tin oxide glass substrate. The electrochemical impedance spectroscopy measurements further confirmed the electron transport differences between DSSCs based on nanosheet/nanoparticle gradient film electrodes and DSSCs based on nanosheet/nanoparticle homogeneous mixtures, pure TiO$_2$ nanoparticles and pure TiO$_2$ nanosheets with the same film thickness.

1. Introduction

The dye-sensitized solar cell, which is regarded as one of the most promising alternatives to the traditional silicon solar cell, has been extensively studied in recent years due to its low cost and possible fabrication of flexible solar cells.[1–10] The heart of the DSSC system is a wide band gap oxide semiconductor film that serves as the support of the dye molecules for light adsorption and electron transportation. Among various oxide semiconductors, nanocrystalline TiO$_2$ has proven to be the most suitable material for solar energy conversion due to its biological and chemical inertness, cost effectiveness, long-term stability against photocorrosion and chemical corrosion.[11–15] Since the morphology, crystal structure and size of TiO$_2$ are crucial factors in determining its chemical, optical and electrochemical performances, different morphological TiO$_2$, such as nanoparticles,[15,16] nanosheets,[17,18] nanotubes,[19,20] nanowires,[21,22] and nanospheres,[23,24] have been fabricated and applied to the photoanode films of the dye-sensitized solar cells (DSSCs).

In general, the high specific surface area, fast electron transport, and excellent light scattering properties play important roles in enhancing the photoelectric conversion efficiency of the DSSCs. Nonetheless, these factors are always incompatible with one another. For example, a conventional photoanode made of 10–20 nanometer-sized TiO$_2$ nanoparticles with a large specific surface area is beneficial for loading abundant dye molecules. However, such sizes are much smaller than the wavelength of visible light and the film is transparent with poor light harvesting. Conversely, the improvement of efficiency by employing large particles (more than 50 nm) with effective light scattering is limited due to the smaller surface area of large particles, which results in poor dye adsorption capacity. To solve this problem, graded photoanode films consisting of TiO$_2$ nanostructures with different sizes or morphologies are expected to accommodate their specific advantages.[25–27] Li *et al.* prepared graded films that were composed of particles with different sizes, and fabricated flexible DSSCs with a light-to-energy conversion efficiency of 3.05%.[25] Wu *et al.* prepared a photoanode with films using hierarchical TiO$_2$ flowers and TiO$_2$ nanoparticles as the overlayer and underlayer, respectively.[26] The DSSCs based on such double layered photoanodes showed a remarkably enhanced power conversion efficiency due to the high specific surface area of the underlayer and pronounced light scattering effects as well as efficient electron transport properties of the overlayer. Lamberti *et al.* fabricated DSSCs based on TiO$_2$ nanotube/nanoparticle composite photoanodes,[27] and found that the obtained photo-conversion efficiency was higher than that of

School of Materials and Energy, Guangdong University of Technology, Guangzhou Higher Education Mega Center 100#, Guangzhou, 510006, P. R. China. E-mail: wenguangwang2005@163.com; hyzhang@gdut.edu.cn; Fax: +86-020-39323232; Tel: +86-020-39323232

nanoparticle-based DSSCs owing to the combined effects of the nanoparticles with a large surface area for dye anchoring and the nanotubes facilitating light harvesting and electron lifetime extension.

Among all kinds of morphologies, 2-dimensional TiO_2 nanosheets with exposed {001} facets have attracted widespread attention as their "high-energy" facets are favorable for more dye adsorption and charge separation.[28,29] Yu *et al.* prepared DSSCs based on anatase TiO_2 nanosheets with exposed {001} facets, which showed enhanced photoelectric conversion performance compared with TiO_2 nanoparticles and commercial-grade Degussa P25 TiO_2 nanoparticle (P25) solar cells.[30] They attributed the enhanced performance to the good crystallization, high pore volume, large particle size and enhanced light scattering of TiO_2 nanosheets. Zhao and coworkers reported the fabrication of DSSCs based on a double light scattering layer film photoelectrode, which showed an enhanced photovoltaic performance due to the relatively high surface area of TiO_2 nanosheet underlayers and enhanced light scattering capability of TiO_2 hollow sphere overlayers.[31]

The functionally graded material (FGM) is an inhomogeneous material with a gradually changing composition and structure of two kinds of materials. This graded structure enables the FGM to have the best advantages of both materials.[32] In the previous research, two kinds of TiO_2 nanostructures with different sizes or morphologies in a photoanode film were homogeneous or in a double-layered mode.[26,27,31] However, in this study, we fabricated a TiO_2 gradient film photoanode with a continuous change of the concentration of nanosheets/nanoparticles perpendicular to the fluorine-doped tin oxide (FTO) glass by a screen printing method. To the best of our knowledge, this is the first time that the preparation of the TiO_2 nanosheet/nanoparticle gradient film photoanode and its application to DSSCs has been reported. The effects of the gradient structure of the photoanode on the performances of the DSSC were investigated and discussed and compared with those of DSSCs based on nanosheets/nanoparticles with homogeneous composition.

2. Experimental

2.1 Preparation of TiO_2 nanosheets

All analytical reagents used in this study were purchased from Tianjin Baishi Chemical Industry Company Limited (China), and were directly used without further purification. The TiO_2 nanosheets were prepared by hydrothermal treatment of a precursor solution containing 50 mL of $Ti(OC_4H_9)_4$ and 6 mL of hydrofluoric acid (with a concentration of 40 wt%) in a Teflon-lined autoclave at 180 °C for 24 h. After hydrothermal reaction, the white precipitates were collected by centrifugation and washed with distilled water and ethanol three times, and finally dried in an oven at 80 °C for 12 h.

2.2 Preparation of TiO_2 paste

The screen printing method is a widespread technique for production of TiO_2 photoanodes due to its fast-printing technique and coating facility with fine control of the position and thickness of the film. Herein, the TiO_2 nanosheet/nanoparticle gradient film was prepared by a screen printing method similar to our recent report.[15] The pastes need to be prepared prior to screen printing. In a typical preparation procedure, 0.5 g of ethyl cellulose (EC) powders were dissolved in 5.7 mL of ethanol to yield a solution with a concentration of 10 wt%. Meanwhile, 4.05 g of terpineol was mixed with 5.2 mL of ethanol, and the resulting mixture was added into the above solution, followed by addition of acetylacetone (0.3 mL) and op emulsifier (0.01 mL). Afterwards, 1 g of TiO_2 powder was added into the above solution. The final mixture was sonicated in an ultrasonic bath for 15 min, and then was put into a thermostatic blender at 80 °C under continuous stirring in order to remove ethanol from the mixed solution. The paste for screen printing was obtained when the weight of the mixture remained unchanged.

2.3 Fabrication of a TiO_2 gradient film electrode

Commercial Degussa P25 TiO_2 (P25) was employed as the source of TiO_2 nanoparticles. The photoanode with TiO_2 nanosheet/nanoparticle gradient concentration from substrate to surface was prepared by a screen printing method using TiO_2 pastes with different nanosheet/nanoparticle mass ratios. To be specific, after one layer of TiO_2 film was printed on the FTO glass (Nippon sheet glass, 14–20 Ω per square), the wet film was kept in air for 10 min and then put into a drying oven at 80 °C for 10 min. After that, repeated printing was carried out to get more layers. A schematic diagram of the TiO_2 nanosheet/nanoparticle gradient film photoanode (denoted as SPG) is shown in Fig. 1. The weight percentages of TiO_2 nanosheets from substrate to surface were varied from 0 to 100%. Two layers were screen-printed on the glass substrate for each percentage of TiO_2 nanosheets. For comparison, TiO_2 films composed of pure nanosheets, pure nanoparticles or a nanosheet/nanoparticle homogeneous mixture with the same printing layers (10 layers) were also fabricated, and the prepared electrodes were labeled as S100, P100 and SPH, respectively. All of the as-prepared films were calcined in a tubular muffle furnace at 450 °C for 30 min with a heating rate of 5 °C min^{-1}. After calcination, the films were cooled down for dye sensitization. Dye sensitization was accomplished by immersing TiO_2 films in anhydrous ethanol solution containing 0.5 mM of N719 dye (purchased from Dalian HeptaChroma SolarTech Co., Ltd. of China) in a sealed beaker at 50 °C for 24 h.[33] Afterwards, the dye-sensitized films were rinsed with ethanol to remove
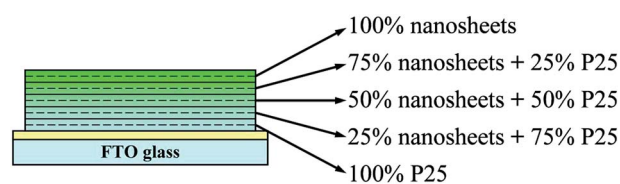

Fig. 1 Schematic diagram of a TiO_2 nanosheet/nanoparticle gradient film photoanode.

physical-adsorbed N719 dye molecules. Finally, the obtained TiO$_2$ film electrodes were dried in an oven at 80 °C for 2 h.

2.4 Characterization

The morphology of the TiO$_2$ nanosheet film on the FTO glass was observed on a JSM-6510 scanning electron microscope (SEM, JEOL, Japan) at an accelerating voltage of 20 kV. The phase structures of the TiO$_2$ film electrodes were obtained on a D/MAX-Ultima IV X-ray diffractometer (XRD, Rigaku, Japan) using Cu Kα irradiation at a scan rate (2θ) of 8° min^{-1}. The accelerating voltage and applied current were 40 kV and 40 mA, respectively. Transmission electron microscopy (TEM) and high-resolution transmission electron microscopy (HRTEM) images were obtained using a Tecnai G20 microscope (USA) with an acceleration voltage of 200 kV. UV-vis diffused reflectance spectra of the photoanodes were recorded using a UV-vis spectrophotometer (UV2450, Shimadzu, Japan). BaSO$_4$ was used as a reflectance standard in a UV-vis diffuse reflectance experiment. The Brunauer–Emmett–Teller (BET) specific surface areas (S_{BET}) of the as-prepared TiO$_2$ nanosheets and P25 as well as the nanosheet/P25 mixture were obtained by nitrogen adsorption–desorption on a Micromeritics ASAP 2020 nitrogen adsorption apparatus (USA). All samples were degassed at 180 °C prior to nitrogen adsorption measurements. The S_{BET} was determined by a multipoint BET method using the adsorption data in the relative pressure P/P_0 range of 0.05–0.25. The desorption isotherm was used to determine the pore size distribution by using the Barret–Joyner–Halender (BJH) method. The photocurrent–voltage I–V characteristic curves were measured using an electrochemical analyzer (CHI660C Instruments) controlled by a computer. A solar simulator (Newport 91160) with an intensity of 100 mW cm^{-2} (1 sun) was employed as the light resource. The active area of DSSCs was 0.14 cm^2. In order to further study the dye-adsorption properties of the TiO$_2$ films with various morphologies and compositions, we immersed the film photoanodes in a desorbent containing 0.1 M of NaOH in water–ethanol (with a volume ratio of 1 : 1) mixed solution to desorb the dye from the photoanode surface and then measured the absorption of the resultant solution on a UV-vis spectrophotometer (UV-2450, Shimadzu, Japan). The concentration of the desorbed dye was calculated by the molar extinction coefficient (1.41 × 10^4 dm^3 mol^{-1} cm^{-1} at 515 nm as reported previously) and absorption.[34]

3.   Results and discussion

The phase structure and crystallite size of TiO$_2$ play an important role in the photoelectric conversion efficiency of DSSCs. Fig. 2 shows the XRD patterns of the FTO glass substrate and TiO$_2$ film photoanodes with different components. Obviously, three strong peaks attributed to SnO$_2$ (JCPDS no. 46-1088) were observed for all XRD curves.[35] For the S100 photoanode, all diffraction peaks except SnO$_2$ peaks can be readily indexed to anatase TiO$_2$ (JCPDS no. 21-1272).[36] In the case of P100 and SPH photoanodes, there is a small amount of rutile phase besides the anatase phase found in them. However, the SPG
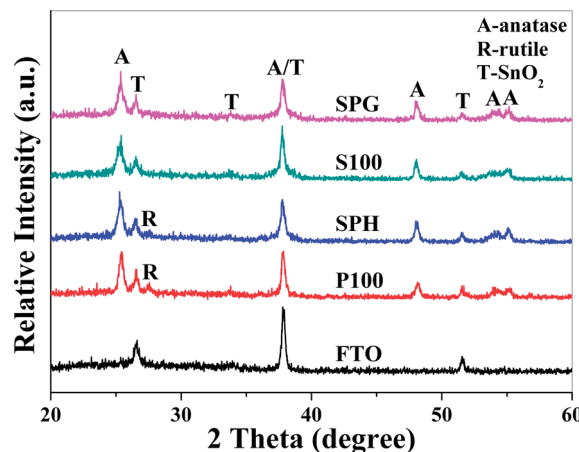

Fig. 2   XRD patterns of a FTO glass substrate (FTO) and TiO$_2$ film photoanodes (P100, SPH, S100 and SPG).

photoanode exhibited the same diffraction peaks as that of the S100 photoanode regardless of a slight difference in intensity and no peaks belonging to the rutile phase were observed. This is due to the fact that the thickness of the nanosheet layer on the outer surface of the SPG film was beyond the scope of XRD analysis, indicating that the film was crack free with few defects.

Fig. 3a and b show the typical SEM images of the surface and cross-sectional morphology of the TiO$_2$ nanosheet/nanoparticle gradient film photoanode. It can be seen from Fig. 3a that the SPG film was relatively uniform and crack free over a large area, which was in good agreement with the XRD analysis. Some macropores and mesopores were observed on the surface of the SPG film. These porous structures would provide an efficient transport pathway for electrolyte molecules in DSSCs. The film thickness with 10 printing layers estimated from Fig. 3b was about 26.6 μm and no obvious boundaries were observed
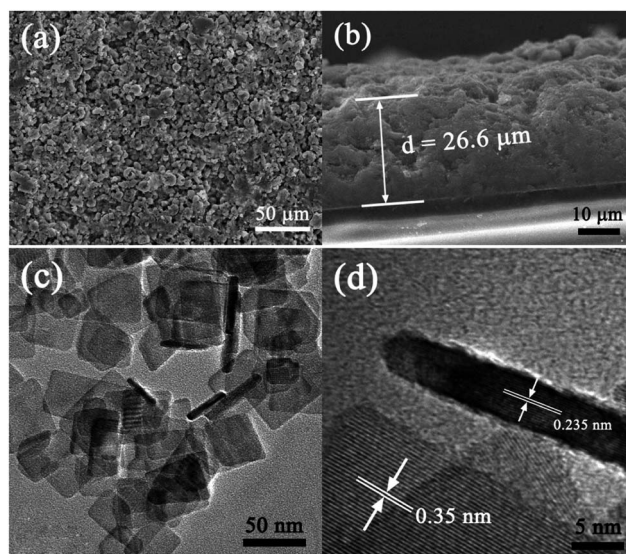

Fig. 3   Surface (a) and cross-sectional (b) SEM images of the SPG film as well as TEM (c) and HRTEM (d) images of TiO$_2$ nanosheets.

between each printing layers, which is favorable for electron transfer amongst the TiO_2 nanosheets and nanoparticles resulting in a low charge recombination rate. The TEM image in Fig. 3c confirms that the prepared nanosheets consist of rectangular sheet-shaped nanostructures with an average side size of about 30–50 nm and a thickness of *ca.* 6.8 nm. The HRTEM image (Fig. 3d) directly shows clear lattice fringes of TiO_2 nanosheets from the side view and top view with lattice spacings of *ca.* 0.235 nm and 0.35 nm, corresponding to the (001) and (101) planes of anatase TiO_2, respectively.[17,37]

Generally, the TiO_2 film with a high specific surface area is beneficial to the adsorption of dye molecules and thus enhances the photoelectric conversion efficiency.[38] A nitrogen adsorption–desorption method was used to investigate the BET surface area and porous structure of the TiO_2 samples with different microstructures. Fig. 4 shows the nitrogen adsorption–desorption isotherms and the corresponding pore size distribution curves (inset) of the TiO_2 nanosheets, TiO_2 nanoparticles as well as the TiO_2 nanosheet/nanoparticle mixture. The mass ratio of nanosheets and nanoparticles in the mixture was 1 : 1. It can be seen from Fig. 4 that all samples have isotherms of type IV (Brunauer–Deming–Deming–Teller classification) and one hysteresis loop at relative high pressures. The hysteresis loop corresponding to TiO_2 nanosheets is of type H3, which can be observed in the slit-like pores.[30] The corresponding pore size distribution curve (inset) shows a peak pore diameter of about 18.6 nm, which is associated with larger pores owing to the aggregation of TiO_2 nanosheets. This corresponds to the observation of TEM images. The hysteresis loop of TiO_2 nanoparticles is of type H2, indicating the presence of ink-like pores.[30] Further observation shows that the isotherm shifts down compared with that of nanosheets, suggesting that the nanoparticles have a lower surface area. The specific surface area of TiO_2 nanosheets is 105 $m^2\,g^{-1}$, which is obviously higher than that of TiO_2 nanoparticles (47 $m^2\,g^{-1}$). Such a high surface area can provide more active sites for the adsorption of dye molecules in DSSCs. The concentrations of N719 dye adsorbed on the surface of P100, SPH, S100 and SPG films were 3.14 × 10^{-4}, 3.98 × 10^{-4}, 4.72 × 10^{-4} and 4.24 × 10^{-4} mol cm^{-2}, respectively. As expected, the S100 film had the highest dye adsorption capacity. Although the SPG film has the same component as the SPH film, more dye molecules were adsorbed on the SPG film than on the SPH film. This may be attributed to the fact that more micropores exist in the SPG film than in the SPH film, which facilitated the dye adsorption. The nanosheet/nanoparticle mixture has a specific surface area of 77 $m^2\,g^{-1}$ between nanosheets and nanoparticles.

Diffuse reflection spectroscopy is a useful measurement for revealing the optical properties of the materials. To investigate the light scattering ability of as-prepared film electrodes, UV-vis diffuse absorption spectra of the P100, SPH, S100 and SPG samples were recorded after dye-sensitization, as shown in Fig. 5. All nanosheet-containing photoanodes exhibited enhanced absorbance in the range of 370 and 750 nm compared with the P100 film electrode. This can be attributed to the high specific surface area of TiO_2 nanosheets which facilitates the adsorption of more dye molecules. The sizes of P25 TiO_2 nanoparticles were in the range of 10 and 25 nm,[30] which were much smaller than the wavelength of visible light. Thus the nanoparticle layer close to the FTO glass substrate was transparent with little light scattering. Especially, the SPG film electrode presented the strongest visible-light absorption, indicating that the nanosheet/nanoparticle gradient film has a much stronger light scattering ability than other films. A schematic diagram of the light scattering effect of the gradient film is shown in Fig. 6. In a testing process of photoelectric performance, the film electrode was irradiated from the side of the glass substrate on which the film was not deposited. When the incident light passed through the FTO glass and contacts with the TiO_2 film electrode, part of the incident light was adsorbed by the nanoparticle layer. It has been reported that the reflectance intensity depends not only on the scattering ability of particles themselves but also the direction of scattering light within the film.[39] With the light penetrating into the deeper layer of the film, the light scattering effect gradually became stronger with increasing content of nanosheets in the gradient
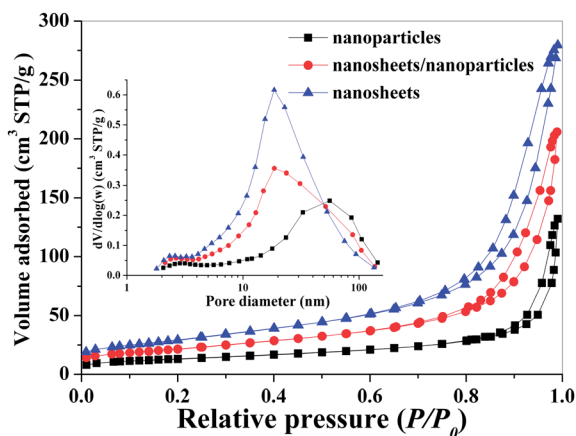

Fig. 4 Nitrogen adsorption–desorption isotherms and the corresponding pore size distribution curves (inset) of the TiO_2 samples with different microstructures.
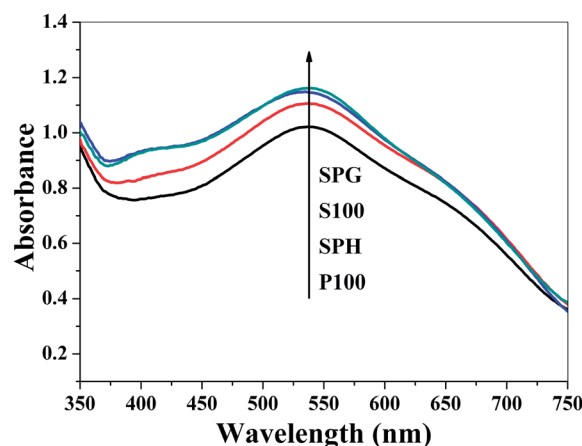

Fig. 5 UV-vis diffuse absorption spectra of the P100, SPH, S100 and SPG film electrodes.
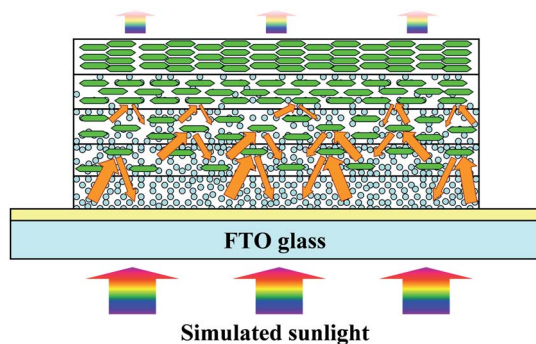
Fig. 6 Schematic diagram of the light scattering effect of the nano-sheet/nanoparticle gradient film.

Table 1 The photovoltaic parameters of the DSSCs made from P100, SPH, S100, and SPG film electrodes

Samples	I_{SC} (mA cm^{-2})	V_{OC} (V)	FF	η (%)
P100	4.7	0.689	0.756	2.45
SPH	9.7	0.663	0.694	4.46
S100	10.6	0.681	0.720	5.20
SPG	13.4	0.679	0.722	6.48

structure. At this time, more light was reflected away from the nanosheet-containing layer and re-adsorbed by the nanoparticle layer. Therefore, the light can be multi-captured within the SPG film electrode, which is beneficial to the incident light harvesting and improvement of photoelectric conversion efficiency of the DSSCs.[40] In the case of the SPH film electrode with a homogeneous mixture of nanosheets and nanoparticles, more incident light can transmit the film resulting in more loss of light. For the S100 film electrode, a certain amount of incident light was reflected away from the electrode without reaching into the deeper layer of the film due to the strong light scattering ability of nanosheets.

Comparison of the I–V characteristics of DSSCs based on P100, SPH, S100, and SPG film electrodes is shown in Fig. 7 and the corresponding short-circuit photocurrent density (I_{SC}), the open-circuit photovoltage (V_{OC}), the fill factor of the cell (FF) and the overall conversion efficiency (η) are listed in Table 1. The solar cell made from the pure TiO$_2$ nanoparticle film electrode (P100) presented the highest V_{OC} and FF due to the fact that the nanoparticle film has better contact with the FTO glass substrate, resulting in the lowest contact resistance. However, the η of such P25-based DSSCs was only 2.45% due to the small surface area and poor light scattering ability of nanoparticles, causing less dye
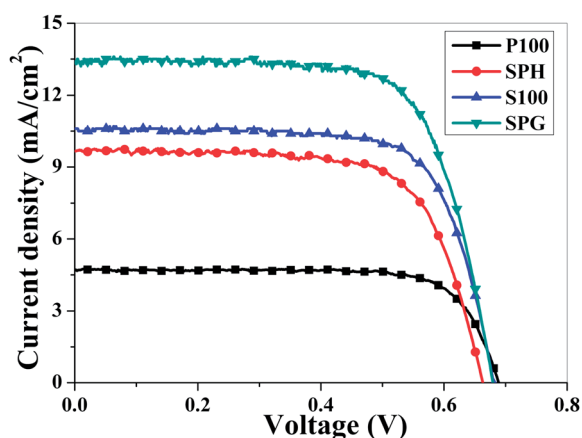
adsorption and poor light harvesting. It has been reported in our previous work that the optimum thickness of the screen-printed film was 11.6 μm.[15] Apparently, in this experiment, the thick film of the P100 electrode impeded the electron transport throughout the film, resulting in a higher recombination rate and shorter lifetime of electrons. In contrast, the SPG solar cell exhibited the highest I_{SC} of 13.4 mA cm^{-2} and η of 6.48%. The η of the SPH and S100 solar cells were 4.46 and 5.2%, respectively. The reasons for the difference of η between four kinds of solar cells were further studied by the following measurements.

To further understand the effect of film structure on the photovoltaic performance of DSSCs, the electrochemical impedance spectroscopy (EIS) measurements were performed to reveal the electron transport during the photovoltaic process of DSSCs. Fig. 8a shows the Nyquist plots of the DSSCs based on
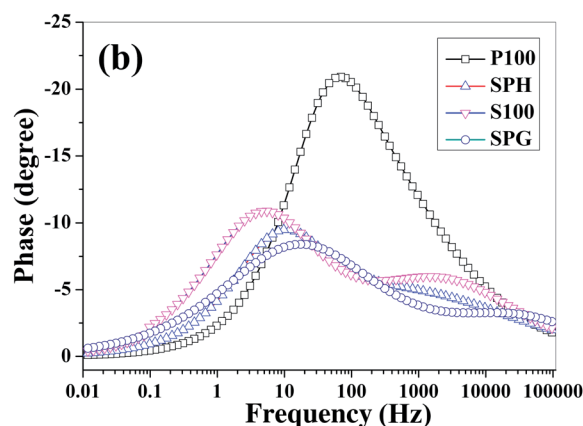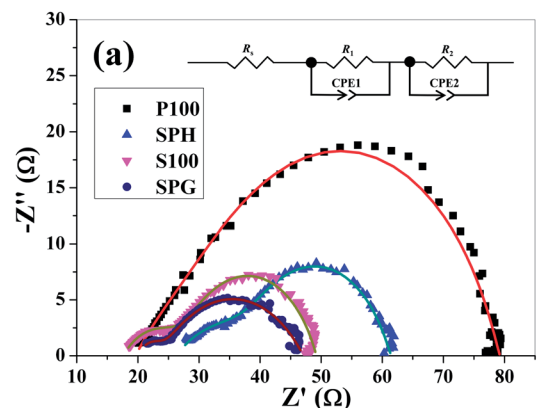

Fig. 7 Comparison of the current–voltage characteristics of DSSCs based on P100, SPH, S100 and SPG film electrodes.

Fig. 8 Nyquist plots (a) and Bode phase plots (b) of DSSCs based on P100, SPH, S100 and SPG film electrodes.

P100, SPH, S100 and SPG film electrodes. Two semicircles including a small one at high frequency and a large one at middle frequency can be observed (Fig. 8a). The Nyquist plots were modeled with an equivalent circuit (inset in Fig. 8a) using non-linear-least-square (NLLS) fit analysis software (Zview software). R_s is attributed to the sheet resistance of the FTO glass substrate and the contact resistance at the FTO/TiO$_2$ interface.[41] The R_s values of DSSCs based on P100, SPH, S100 and SPG electrodes calculated according to the equivalent circuit were 19.6, 26.25, 17.75, and 19.99 Ω, respectively. It is clear that the S100 film electrode has the smallest R_s, implying better electronic contact between nanosheets and FTO glass due to less defects existing in TiO$_2$ nanosheets than in nanoparticles, as shown in Fig. 9.[42,43] The R_s of the P100 cell was almost the same as that of the SPG cell owing to the good contact between the compact TiO$_2$ nanoparticle layer and FTO substrate. However, too many holes or defects existing between TiO$_2$ nanosheets and nanoparticles lead to poor electronic contact between the SPH film and FTO glass (see Fig. 9), resulting in the largest R_s of the SPH cell. The small semicircle in the high frequency region is related to the charge transfer resistance (R_1) and interfacial capacitance (CPE1) at the interfaces between the electrolyte and Pt electrode.[44] The large semicircle in the middle frequency region is related to the electron transport resistance (R_2) within the TiO$_2$ film and interfacial capacitance (CPE2) at the TiO$_2$/dye/electrolyte interface.[41] The R_2 plays a vital role in the photovoltaic performance of the DSSC in that it is related to the number of electrons going back to the electrolyte at the TiO$_2$/electrolyte interface.[41] The R_2 values of DSSCs based on P100, SPH, S100 and SPG electrodes calculated according to the equivalent circuit were 42.04, 22.98, 20.11 and 23.34 Ω, respectively. A schematic diagram of the electron transfer within the TiO$_2$ films is shown in Fig. 9. The largest R_2 for the P100 electrode can be explained that a lot of grain boundaries between TiO$_2$ nanoparticles prevented photoelectrons from transferring smoothly through the film, and many electrons were lost at the grain

boundary without reaching the external circuit.[41] However, the S100 electrode exhibited the smallest R_2 due to the fact that the TiO$_2$ nanosheets with high crystallinity provide the shortest pathway for electron transfer.[44] The fast transfer of photoelectrons from the TiO$_2$ film to FTO glass reduced the recombination and back reactions of electrons with I$_3^-$. Moreover, the TiO$_2$ nanosheets throughout the film also resulted in the smaller R_2 of the SPH electrode. The R_2 value of DSSCs based on the SPG electrode was between that of P100 and SPH electrodes. Bode phase plots of EIS can offer the lifetime information of electrons during the photovoltaic process and are shown in Fig. 8b. The electron lifetime (τ_e) can be calculated according to the equation $\tau_e = 1/2\pi f_{max}$, where f_{max} is the maximum frequency of the peak in the intermediate frequency region.[45,46] The τ_e values of DSSCs based on P100, SPH, S100 and SPG electrodes were calculated to be 2.28, 16.3, 29.0 and 9.15 ms, respectively. The longer τ_e means the lower recombination rate of electrons during the electron transfer across the TiO$_2$ film,[47] which was in good agreement with the analysis of R_2. Although the SPG cell had an τ_e shorter than that of SPH and S100 cells, it exhibited the highest I_{SC} and η among four kinds of solar cells. Therefore, it is the strong light scattering ability of nanosheet/nanoparticle gradient structure which predominates over the negative influence of larger charge transfer resistance that contributes to the highest photoelectric performance of the SPG solar cell.

On the basis of the above experimental results, the enhanced conversion efficiency of the SPG solar cell can be attributed to the combined effects of several factors: firstly, the nanosheet/nanoparticle gradient structures have a strong light scattering effect that enables the incident light to be multi-reflected within the film, effectively prolonging the optical distance and enhances light harvesting and photocurrent density. Secondly, the TiO$_2$ nanoparticle underlayers of the nanosheet/nanoparticle gradient film ensured better electronic contact with the FTO glass, which resulted in the lower contact resistance and higher photovoltage. Thirdly, the relatively higher specific surface area of nanosheets and nanoparticles was in favor of the dye absorption. Undoubtedly, the DSSCs based on the SPG photoanode exhibited the highest photoelectric conversion efficiency. The gradient structure of the film electrode showed a significant influence on the photovoltaic performance of the DSSCs, suggesting that the conversion efficiency can be further improved by careful design of the photoanode structure.
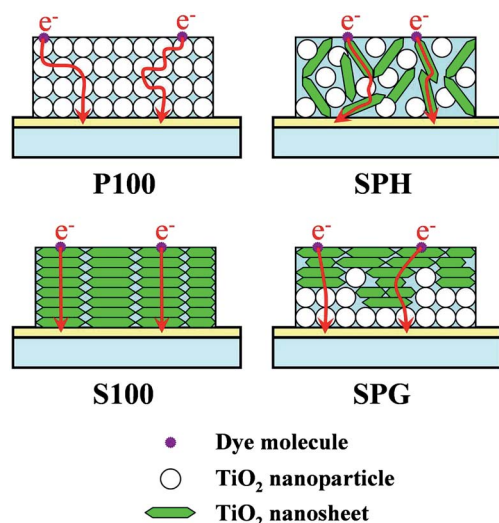
4. Conclusions

In summary, a TiO$_2$ film photoanode with nanosheet/nanoparticle gradient structure was prepared by a screen printing method and assembled into a solar cell. Meanwhile, TiO$_2$ films based on nanosheet/nanoparticle homogeneous mixtures, pure TiO$_2$ nanoparticles and pure TiO$_2$ nanosheets with the same film thickness were also prepared for comparison. The gradient structure of the photoanode showed a remarkable influence on the photovoltaic properties of the DSSC, which exhibited the highest photoelectric conversion efficiency of 6.48%. The enhanced performance can be attributed to the strong light scattering ability of the gradient structure and good electronic

Fig. 9 Schematic diagram of the electron transport within the TiO$_2$ films of P100, SPH, S100 and SPG electrodes.

contact between the TiO$_2$ nanoparticle underlayer and FTO glass. This investigation may open up an alternative avenue for fabrication and structural design of DSSCs with higher photo-electric conversion efficiency.

Acknowledgements

References

1 C. P. Cho, C. C. Chu, W. T. Chen, T. C. Huang and Y. T. Tao, *J. Mater. Chem.*, 2012, **22**, 2915–2921.

2 P. K. Santra and P. V. Kamat, *J. Am. Chem. Soc.*, 2012, **134**, 2508–2511.

3 S. I. Cha, Y. Kim, K. H. Hwang, Y. Shin, S. H. Seo and D. Y. Lee, *Energy Environ. Sci.*, 2012, **5**, 6071–6075.

4 J. H. Im, C. R. Lee, J. W. Lee, S. W. Park and N. G. Park, *Nanoscale*, 2011, **3**, 4088–4093.

5 Q. F. Zhang and G. Z. Cao, *Nano Today*, 2011, **6**, 91–109.

6 Y. P. Fu, M. Peng, Z. B. Lv, X. Cai, S. C. Hou, H. W. Wu, X. Yu, H. Kafafy and D. C. Zou, *Nano Energy*, 2013, **2**, 537–544.

7 J. H. Wu, Y. M. Xiao, G. T. Yue, Q. W. Tang, J. M. Lin, M. L. Huang, Y. F. Huang, L. Q. Fan, Z. Lan, S. Yin and T. Sato, *Adv. Mater.*, 2012, **24**, 1884–1888.

8 J. Y. Liu, D. F. Zhou, M. F. Xu, X. Y. Jing and P. Wang, *Energy Environ. Sci.*, 2011, **4**, 3545–3551.

9 J. Y. Liao, J. W. He, H. Y. Xu, D. B. Kuang and C. Y. Su, *J. Mater. Chem.*, 2012, **22**, 7910–7918.

10 B. Liu and E. S. Aydil, *J. Am. Chem. Soc.*, 2009, **131**, 3985–3990.

11 E. J. W. Crossland, N. Noel, V. Sivaram, T. Leijtens, J. A. Alexander-Webber and H. J. Snaith, *Nature*, 2013, **495**, 215–219.

12 Y. L. Wang, W. G. Yang and W. M. Shi, *Ind. Eng. Chem. Res.*, 2011, **50**, 11982–11987.

13 K. Fan, C. Q. Gong, T. Y. Peng, J. N. Chen and J. B. Xia, *Nanoscale*, 2011, **3**, 3900–3906.

14 J. J. Fan, S. W. Liu and J. G. Yu, *J. Mater. Chem.*, 2012, **22**, 17027–17036.

15 H. Y. Zhang, W. G. Wang, H. Liu, R. Wang, Y. M. Chen and Z. W. Wang, *Mater. Res. Bull.*, 2014, **49**, 126–131.

16 C. P. Hsu, K. M. Lee, J. T. W. Huang, C. Y. Lin, C. H. Lee, L. P. Wang, S. Y. Tsai and K. C. Ho, *Electrochim. Acta*, 2008, **53**, 7514–7522.

17 B. Laskova, M. Zukalova, L. Kavan, A. Chou, P. Liska, Z. Wei, L. Bin, P. Kubat, E. Ghadiri, J. E. Moser and M. Grätzel, *J. Solid State Electrochem.*, 2012, **16**, 2993–3001.

18 J. Zhang, J. Wang, Z. Zhao, T. Yu, J. Feng, Y. Yuan, Z. Tang, Y. Liu, Z. Li and Z. Zou, *Phys. Chem. Chem. Phys*, 2012, **14**, 4763–4769.

19 X. Luan, D. S. Guan and Y. Wang, *J. Phys. Chem. C*, 2012, **116**, 14257–14263.

20 P. Roy, D. Kim, K. Lee, E. Spiecker and P. Schmuki, *Nanoscale*, 2010, **2**, 45–59.

21 J. Y. Liao, B. X. Lei, H. Y. Chen, D. B. Kuang and C. Y. Su, *Energy Environ. Sci.*, 2012, **5**, 5750–5757.

22 A. Kumar, A. R. Madaria and C. W. Zhou, *J. Phys. Chem. C*, 2010, **114**, 7787–7792.

23 J. T. Park, D. K. Roh, W. S. Chi, R. Patel and J. H. Kim, *J. Ind. Eng. Chem.*, 2012, **18**, 4449–4455.

24 Y. J. Kim, M. H. Lee, H. J. Kim, G. Lim, Y. S. Choi, N. G. Park, K. Kim and W. I. Lee, *Adv. Mater.*, 2009, **21**, 1–6.

25 X. Li, H. Lin, J. B. Li, N. Wang, C. F. Lin and L. Z. Zhang, *J. Photochem. Photobiol., A*, 2008, **195**, 247–253.

26 W. Q. Wu, Y. F. Xu, H. S. Rao, C. Y. Su and D. B. Kuang, *Nanoscale*, 2013, **5**, 4362–4369.

27 A. Lamberti, A. Sacco, S. Bianco, M. Quaglio, D. Manfredi and C. F. Pirri, *Microelectron. Eng.*, 2013, **111**, 137–142.

28 X. Wu, G. Q. Lu and L. Z. Wang, *J. Mater. Res.*, 2013, **28**, 475–479.

29 W. G. Yang, J. M. Li, Y. L. Wang, F. Zhu, W. M. Shi, F. R. Wan and D. S. Xu, *Chem. Commun.*, 2011, **47**, 1809–1811.

30 J. G. Yu, J. J. Fan and K. L. Lv, *Nanoscale*, 2010, **2**, 2144–2149.

31 L. Zhao, J. Li, Y. Shi, S. M. Wang, J. H. Hu, B. H. Dong, H. B. Lu and P. Wang, *J. Alloys Compd.*, 2013, **575**, 168–173.

32 F. Capasso, *Annu. Rev. Mater. Sci.*, 1986, **16**, 263–291.

33 J. J. Fan, W. Q. Cai and J. G. Yu, *Chem.–Asian J.*, 2011, **6**, 2481–2490.

34 Z. S. Wang, H. Kawauchi, T. Kashima and H. Arakawa, *Coord. Chem. Rev.*, 2004, **248**, 1381–1389.

35 W. Q. Wu, B. X. Lei, H. S. Rao, Y. F. Xu, Y. F. Wang, C. Y. Su and D. B. Kuang, *Sci. Rep.*, 2013, **3**, 1352.

36 W. G. Wang, J. G. Yu, Q. J. Xiang and B. Cheng, *Appl. Catal., B*, 2012, **119**, 109–116.

37 J. G. Yu, W. G. Wang, B. Cheng and B. L. Su, *J. Phys. Chem. C*, 2009, **113**, 6743–6750.

38 D. Cahen, G. Hodes, M. Grätzel, J. F. Guillemoles and I. Riess, *J. Phys. Chem. B*, 2000, **104**, 2053–2059.

39 B. Munkhbayar, M. Dorjderem, D. Sarangerel and B. Ochirkhuyag, *Nanosci. Nanotechnol. Lett.*, 2013, **5**, 741–749.

40 J. G. Yu, Q. L. Li and Z. Shu, *Electrochim. Acta*, 2011, **56**, 6293–6298.

41 T. Hoshikawa, M. Yamada, R. Kikuchi and K. Eguchi, *J. Electrochem. Soc.*, 2005, **152**, E68–E73.

42 Z. Y. Wang, K. L. Lv, G. H. Wang, K. J. Deng and D. G. Tang, *Appl. Catal., B*, 2010, **100**, 378–385.

43 Y. Zheng, K. L. Lv, Z. Y. Wang, K. J. Deng and M. Li, *J. Mol. Catal. A: Chem.*, 2012, **356**, 137–143.

44 Z. Y. Gao, Z. L. Wu, X. M. Li, J. L. Chang, D. P. Wu, P. F. Ma, F. Xu, S. Y. Gao and K. Jiang, *CrystEngComm*, 2013, **15**, 3351–3358.

45 Y. M. Feng, F. Wu, J. Jiang, J. H. Zhu, G. J. Fodjouong, G. X. Meng, Y. M. Xing, W. W. Wang and X. T. Huang, *J. Alloys Compd.*, 2013, **581**, 610–615.

46 J. T. Park, D. K. Roh, R. Patel, E. Kim, D. Y. Ryu and J. H. Kim, *J. Mater. Chem.*, 2010, **20**, 8521–8530.

47 J. Bisquert, F. Fabregat-Santiago, I. Mora-Seró, G. Garcia-Belmonte and S. Giménez, *J. Phys. Chem. C*, 2009, **113**, 17278–17290.